Volume 1 | Number 1 | Jan 2013 | Pages 1–100

Nanoscale

www.rsc.org/nanoscale

ROYAL SOCIETY OF CHEMISTRY

ROYAL SOCIETY OF CHEMISTRY

www.rsc.org/nanoscale

Strong Correlation between Early Stage Atherosclerosis and Electromechanical Coupling of Aorta

X.Y. Liu [1,*], F. Yan [2,4,*], L.L. Niu[2,4], Q.N. Chen[3], H.R. Zheng [2,4,#], and J.Y. Li [3,4,#]

[1]   College of Metallurgy and Materials Engineering, Chongqing Key Laboratory of Nano/Micro Composites and Devices, Chongqing University of Science & Technology, Chongqing, China

[2]   Paul C. Lauterbur Research Center for Biomedical Imaging, Institute of Biomedical and Health Engineering, Shenzhen Institutes of Advanced Technology, Chinese Academy of Sciences, Shenzhen, China

[3]   Department of Mechanical Engineering, University of Washington, Seattle, WA, USA

[4]   Shenzhen Key Laboratory of Nanobiomechanics, Shenzhen Institutes of Advanced Technology, Chinese Academy of Sciences, Shenzhen, China

[*]   X.Y. Liu and F. Yan contributed equally to this work

[#]   Authors to whom the correspondence should be addressed to; Email: jjli@uw.edu and hr.zheng@siat.ac.cn

ABSTRACT

Atherosclerosis is the underlying cause of cardiovascular diseases that are responsible for many deaths in the world, and the early diagnosis of atherosclerosis is highly desirable. The existing imaging methods, however, are not capable of detecting the early stage of atherosclerosis development due to their limited spatial resolution. Using piezoresponse force microscopy (PFM), we show that the piezoelectric response of an aortic wall increases as atherosclerosis advances, while the stiffness of the aorta shows a less evident correlation with atherosclerosis. Furthermore, we show that there is strong correlation between the coercive electric field necessary to switch the polarity of artery and the development of atherosclerosis. Thus by measuring the electromechanical coupling of aortic wall, it is possible to probe atherosclerosis at the early stage of its development, not only improving the spatial resolution by orders of magnitude, but also providing comprehensive quantitative information on biomechanical properties of artery.

Atherosclerosis is the underlying cause of cardiovascular diseases [1] that are the leading cause of death in the world [2]. It is widely recognized as a chronic immune-inflammatory disease, and the development fall into three stages [3]. Although recent researches highlight important cell biological atherogenic processes, and there are considerable interests in understanding and diagnosing atherosclerosis at the early stage of its development, it is still rather difficult to distinguish between lesion initiation and progression [4]. Traditionally, diagnosis of atherosclerosis was possible only at advanced stages of disease, and there are now a number of imaging techniques developed to visualize atherosclerosis in both clinical and research laboratories [5-8], including ultrasound based techniques such as B-mode ultrasonography [5,6], optical imaging techniques such as near-infrared fluorescence reflectance or fluorescence molecular tomography [7,8], magnetic resonance imaging [9], single photonemission-computed tomography and positron emission tomography [10], and optimal coherence tomography [11] that can be used with spectroscopic techniques such as elastography to assess biomechanical properties of arteries [12]. With spatial resolution no better than 10 μm, these existing imaging techniques are not capable of detecting small changes in structures and properties of aorta during the early stage of atherosclerosis development.

In this work, we use piezoresponse force microscopy (PFM) [13,14] as a highly sensitive tool for early probing of atherosclerosis with nanometer resolution and quantitative information, and the imaging is based on the electromechanical coupling of aortic wall, a well-known phenomenon that exists in many biological tissues [15-25]. It has been widely speculated that such electromechanical coupling possesses important physiological significance [26-28], and we show that the electromechanical response of aortic wall indeed evolve with atherosclerosis development, making the probing of early stage development possible.

Our method is based on the piezoelectricity of aortic wall [20,29], which deforms under an external electric field. Aorta samples from wide type mice and APoE-/- mice fed with a chow diet for 24 weeks, and APoE-/- mice fed with a high-fat diet for 24 weeks have been prepared, and these mice are also on the C57BL/6J background. The detailed description on Materials and Methods can be found in the Supplementary Materials. Atherosclerotic plaques typically occur in the aortic, coronary, carotid, and cerebral arteries and are closely associated with high incidences of

cardiovascular disease and stroke [32,33]. Deletion of APoE gene in mice leads to development of atherosclerotic lesions in the aorta and its branches due to disturbed flow and increased plasma levels of low-density lipoprotein [34,35], and this is the reason that we selected these mouse aorta to examine in our study. In order to identify the plaque region on the sample, we use oil red O to stain these arteries. Indeed, for APoE-/- mice fed with a high-fat diet, plaque has been developed (Figure S1, Supplementary Materials), and samples of aortic wall have been taken on the spot of plaque as well as away from it. This results in four different types of samples: aorta from C57BL/6J wide type mouse fed with chow diet (group 1), APoE-/- mouse fed with chow diet (group 2), APoE-/- mouse fed with high fat diet, in the plaque-free region (group 3), and APoE-/- mouse fed with high fat diet, in the plaque region (group 4). The representative microscopic images from the mouse aorta sections after staining with hematoxylin and eosin (H&E) dyes are shown in Figure 1a. In the aortal samples from wide type mice (group 1) and APoE-/- mice fed with chow diet (group 2), the thickness of vein wall was normal and uniform. In addition, the aorta sample from the plaque-free region in APoE-/- mice fed with high fat diet (group 3) also have the uniform thickness of vein wall. On the other hand, the aorta sample taken from the plaque region in APoE-/- mice fed with high fat diet (group 4) has nonuniform thickness of vein wall with obvious thickened intima structure, showing the visible atherosclerotic lesions in the same animal. Furthermore, a significantly higher expression of a-smooth muscle actin (α-SMA, a VSMC-specific marker for atherosclerotic lesions) was observed in the aorta of APoE-/- mice fed with high fat diet than that of wide type mice or APoE-/- mice fed with chow diet (Figure 1b), indicating that a faster development of atherosclerotic lesions in the APoE-/- mice fed with high fat diet. It is worth noting that there is no significant difference in (H&E) staining images among these samples, except for the sample taken from plaque-region (group 4), suggesting that the traditional histochemical staining techniques are incapable of detecting early development of atherosclerosis.

We then probed the four groups of destained aorta samples using PFM, hoping to achieve higher spatial resolution and sensitivity. The principle of PFM as well as typical data are shown in Figure S2, suggesting that the cantilever-sample system can be modeled as a damped driven harmonic oscillator [30,31], which fits the measured amplitude-frequency and phase-frequency data well. This enables us to determine not only the intrinsic PFM response corrected using damped driven harmonic oscillator model, but also the resonant frequency of the system that correlates

with the stiffness of the sample. The topographic mappings have been obtained simultaneously (Figure S3), showing the surface roughness of the samples in the range of 125-258 nm with no clear differences among different groups. We first examine the corrected vertical PFM amplitude of these four different groups of mouse samples (Figure 2a), and the contrast is evident: APoE-/- mice have higher PFM amplitude than wide type, while APoE-/- mice fed with high-fat diet has higher PFM amplitude than that fed with chow diet. Furthermore, for APoE-/- mice fed with high-fat diet, sample from plaque region have higher PFM amplitude than sample from the plaque-free region. Such difference can be made clearer by comparing the histograms of PFM amplitude distributions of these four types of samples (Figure 2b), and the increasing trend from wide type mice to APoE-/- mice, from chow diet to high-fat diet, and from plaque-free region to plaque region is evident. This suggest that there could be a strong correlation between atherosclerosis development and electromechanical response of aortic wall, since both APoE gene deficiency and high-fat diet favor atherosclerosis development.

In order to make sure that the contrasts seen in Figure 2 have statistical significance, we have analyzed 12 samples from each group of tissues, yielding 48 mappings of corrected PFM amplitude and thus 48 histograms. Each histogram is then converted into a one-dimensional mapping, with color code representing its intensity. These color mappings are grouped together by tissue types (Figure 3a), and the increasing trend from wide type mice to APoE-/- mice , from chow diet to high-fat diet, and from the plaque-region to plaque region is confirmed, suggesting that there is a strong correlation between atherosclerosis development and electromechanical response of aortic wall. Furthermore, we have also mapped the variation of resonant frequency that correlates with sample stiffness, since atherosclerosis development is often associated with hardening of artery. The increasing trend of resonant frequency is still observed (Figure 3b), but to a much less extent, suggesting that the electromechanical response is more sensitive to atherosclerosis development than stiffness. Both peak and mean values of corrected amplitude and resonant frequency for each groups of samples are summarized in Table 1, and statistics analysis shows that both the peak value and mean value of corrected PFM amplitude were significantly different when comparing with each group ($p < 0.05$). As for the peak value of resonant frequency, the significant differences exist between group 1 and group 3, group 1 and group 4, group 2 and group 4, and group 3 and group 4 ($p < 0.05$). For the mean value of resonant frequency, the significant differences exist between group 2 and group 4, as well as

between group 3 and group 4. These again suggest that electromechanical is a more sensitive measure that correlates with the atherosclerosis development, while stiffness, or resonant frequency, is less reliable, especially during the early stage of atherosclerosis development. Comparison of typical resonant frequency mapping and corresponding histogram are shown in Figure S4.

Furthermore, it has been shown that the polarity of electromechanical response of aortic wall can be switched by external electric field [20], triggered by the DC voltage applied through conductive SPM probe on top of AC voltage (Figure 4a). When the polarity is switched, hysteresis loop between PFM phase and applied DC voltage can be obtained (Figure 4b). Interestingly, clear contrast in coercive voltage, the threshold voltage that is necessary to switch the polarity of the sample, is observed among these four different groups of samples. With atherosclerosis development, the coercive voltage increases, until the plaque develops, on top of which the coercive voltage drops substantially. Such trend is seen more clearly in the bar column comparison (Figure 4c), again suggesting a strong correlation between electromechanical responses and atherosclerosis development. The polarity of the sample is getting increasingly more difficult to switch, until the plaque is developed, wherein the deposition of lipids or small polar molecules makes it easier to switch [36-38]. As such, the coercive voltage offers additional measure that correlates with atherosclerosis development well. Detailed statistical comparison can be found in Table 2. Obviously, there are significantly different coercive voltages in four different groups of samples. The coercive voltage of aorta samples from group 1 is 2.80 ± 1.75 V, much lower than that of samples from group 2 with 8.60 ± 2.43 V (P < 0.001). The aorta sample from group 3 has the highest coercive voltage with 19.82 ± 7.42 V, about 7.08- and 2.30-fold higher than that of samples from group 1 and group 2 (P < 0.001). Interestingly, the coercive voltage of aorta samples from group 4 drops substantially, reaching 1.42 ± 0.74 V, which we believe is due to the deposition of small polar molecules in the plaque region. The histogram distributions of coercive voltage for these four groups of samples are shown in Fig. S5, where the difference among different groups is evident as well.

Thus by using highly sensitive PFM techniques, local electromechanical response of aortic wall as small as picometer can be measured with nanometer resolution, making it possible to detect tiny changes in the structures and properties of artery at the early stage of atherosclerosis. In

particular we show that for aorta samples from different groups of mice at different stages of atherosclerosis development, there are strong statistical difference in measured piezoresponse, where the PFM amplitude increases as atherosclerosis advances. In contrast, for the resonant frequency measured, which is related with the contact stiffness of the sample, the correlation is less evident. Furthermore, we show that the critical electric field necessary to switch the polarity of the aortic wall also vary as the atherosclerosis advances. We note that the piezoelectricity in biological tissues is quite universal and relatively well understood [26], and recent molecular dynamics (MD) simulation on tropoelastin revealed that the phenomenon arises from the intrinsic dipole possessed by the biomolecules [39]. The mechanism responsible for the observed correlation, however, is not yet clear and requires further investigation, though it is plausible that it is induced by the subtle structure change of aortic wall associated with atherosclerosis development. Similar effects have also been observed in elastin treated by glucose [40], and it might be related to the membrane activity at the level of ionic channels that exhibit ferroelectric-like behavior as well [41]. We should also point out that this technique is currently limited to ex-vivo laboratory use, though we believe it can be used as a powerful research tool to study the development of atherosclerosis as well as the effectiveness of early intervention strategies. By the time that atherosclerosis is detected by conventional imaging techniques, it is already too late to reverse the process. However, if we can detect the early stage of atherosclerosis development, then various early intervention strategies can be attempted and evaluated, and it is conceivable to stop and even reverse the advance of atherosclerosis at such early stage.

REFERENCES

1.   Lusis, A.J. Atherosclerosis. *Nature* **407**, 233-241 (2000).
2.   Weber, C. & Noels, H. Atherosclerosis: current pathogenesis and therapeutic options. *Nat Med* **17**, 1410-1422 (2011).
3.   Libby, P., Ridker, P.M. & Hansson, G.K. Progress and challenges in translating the biology of atherosclerosis. *Nature* **473**, 317-325 (2011).
4.   Nakashima, Y., Wight, T.N. & Sueishi, K. Early atherosclerosis in humans: role of diffuse intimal thickening and extracellular matrix proteoglycans. *Cardiovasc Res* **79**, 14-23 (2008).
5.   Lindsay, A.C. & Choudhury, R.P. Form to function: current and future roles for atherosclerosis imaging in drug development. *Nature Reviews Drug Discovery* **7**, 517-529 (2008).
6.   De Groot, E.*, et al.* Measurement of carotid intima–media thickness to assess progression and regression of atherosclerosis. *Nature clinical practice Cardiovascular medicine* **5**, 280-288 (2008).

7.   Choudhury, R.P. & Fisher, E.A. Molecular imaging in atherosclerosis, thrombosis, and vascular inflammation. *Arteriosclerosis, thrombosis, and vascular biology* **29**, 983-991 (2009).

8.   Jaffer, F.A., Libby, P. & Weissleder, R. Optical and multimodality molecular imaging insights into atherosclerosis. *Arteriosclerosis, thrombosis, and vascular biology* **29**, 1017-1024 (2009).

9.   Makowski, M.R. & Botnar, R.M. MR imaging of the arterial vessel wall: molecular imaging from bench to bedside. *Radiology* **269**, 34-51 (2013).

10.   Yankeelov, T.E., Abramson, R.G. & Quarles, C.C. Quantitative multimodality imaging in cancer research and therapy. *Nature Reviews Clinical Oncology* **11**, 670-680 (2014).

11.   Sinclair, H., Bourantas, C., Bagnall, A., Mintz, G.S. & Kunadian, V. OCT for the Identification of Vulnerable Plaque in Acute Coronary Syndrome. *JACC: Cardiovascular Imaging* **8**, 198-209 (2015).

12.   Rogowska, J., Patel, N., Fujimoto, J. & Brezinski, M. Optical coherence tomographic elastography technique for measuring deformation and strain of atherosclerotic tissues. *Heart* **90**, 556-562 (2004).

13.   Bonnell, D.A., Kalinin, S.V., Kholkin, A. & Gruverman, A. Piezoresponse force microscopy: a window into electromechanical behavior at the nanoscale. *Mrs Bull* **34**, 648-657 (2009).

14.   Li, J., Li, J.-F., Yu, Q., Chen, Q.N. & Xie, S. Strain-based scanning probe microscopies for functional materials, biological structures, and electrochemical systems. *Journal of Materiomics* **1**, 3-21 (2015).

15.   Fukada, E. & Yasuda, I. On the piezoelectric effect of bone. *J Phys Soc Jpn* **12**, 1158-1162 (1957).

16.   Halperin, C.*, et al.* Piezoelectric effect in human bones studied in nanometer scale. *Nano Letters* **4**, 1253-1256 (2004).

17.   Kalinin, S.V., Rodriguez, B.J., Jesse, S., Thundat, T. & Gruverman, A. Electromechanical imaging of biological systems with sub-10 nm resolution. *arXiv preprint cond-mat/0504232* (2005).

18.   Minary-Jolandan, M. & Yu, M.-F. Uncovering nanoscale electromechanical heterogeneity in the subfibrillar structure of collagen fibrils responsible for the piezoelectricity of bone. *ACS nano* **3**, 1859-1863 (2009).

19.   Harnagea, C.*, et al.* Two-dimensional nanoscale structural and functional imaging in individual collagen type I fibrils. *Biophys J* **98**, 3070-3077 (2010).

20.   Liu, Y., Zhang, Y., Chow, M.-J., Chen, Q.N. & Li, J. Biological ferroelectricity uncovered in aortic walls by piezoresponse force microscopy. *Phys Rev Lett* **108**, 078103 (2012).

21.   Heredia, A.*, et al.* Nanoscale Ferroelectricity in Crystalline γ-Glycine. *Adv Funct Mater* **22**, 2996-3003 (2012).

22.   Li, T. & Zeng, K. Nanoscale piezoelectric and ferroelectric behaviors of seashell by piezoresponse force microscopy. *J Appl Phys* **113**, 187202 (2013).

23.   Zhou, X., Miao, H. & Li, F. Nanoscale structural and functional mapping of nacre by scanning probe microscopy techniques. *Nanoscale* **5**, 11885-11893 (2013).

24.   Bystrov, V., Seyedhosseini, E., Kopyl, S., Bdikin, I. & Kholkin, A. Piezoelectricity and ferroelectricity in biomaterials: Molecular modeling and piezoresponse force microscopy measurements. *J Appl Phys* **116**, 066803 (2014).

25.   Denning, D.*, et al.* Piezoelectricity in collagen type II fibrils measured by scanning probe microscopy. *J Appl Phys* **116**, 066818 (2014).

26.   Shamos, M.H. Piezoelectricity as a fundamental property of biological tissues. *Nature* **213**, 267-269 (1967).

27.   Lang, S.B. Piezoelectricity, pyroelectricity and ferroelectricity in biomaterials: Speculation on their biological significance. *Dielectrics and Electrical Insulation, IEEE Transactions on* **7**, 466-473 (2000).

28.   Liu, Y.*, et al.* Ferroelectric switching of elastin. *Proceedings of the National Academy of Sciences* **111**, E2780-E2786 (2014).

29.   Fukada, E. & Hara, K. Piezoelectric effect in blood vessel walls. *J Phys Soc Jpn* **26**, 777-780 (1969).
30.   Gannepalli, A., Yablon, D., Tsou, A. & Proksch, R. Mapping nanoscale elasticity and dissipation using dual frequency contact resonance AFM. *Nanotechnology* **22**, 355705 (2011).
31.   Xie, S.*, et al.* High resolution quantitative piezoresponse force microscopy of BiFeO 3 nanofibers with dramatically enhanced sensitivity. *Nanoscale* **4**, 408-413 (2012).
32.   Sakakura, K.*, et al.* Pathophysiology of atherosclerosis plaque progression. *Heart, Lung and Circulation* **22**, 399-411 (2013).
33.   Katsanos, A.H.*, et al.* Complex Atheromatous Plaques in the Descending Aorta and the Risk of Stroke A Systematic Review and Meta-Analysis. *Stroke* **45**, 1764-1770 (2014).
34.   Johnson, J.L. & Jackson, C.L. Atherosclerotic plaque rupture in the apolipoprotein E knockout mouse. *Atherosclerosis* **154**, 399-406 (2001).
35.   Hofker, M.H., van Vlijmen, B.J. & Havekes, L.M. Transgenic mouse models to study the role of APOE in hyperlipidemia and atherosclerosis. *Atherosclerosis* **137**, 1-11 (1998).
36.   Bleich, H.L., Boro, E.S. & Small, D.M. Cellular mechanisms for lipid deposition in atherosclerosis. *New Engl J Med* **297**, 873-877 (1977).
37.   Brown, M.S. & Goldstein, J.L. Lipoprotein metabolism in the macrophage: implications for cholesterol deposition in atherosclerosis. *Annu Rev Biochem* **52**, 223-261 (1983).
38.   Tabas, I., Williams, K.J. & Borén, J. Subendothelial lipoprotein retention as the initiating process in atherosclerosis update and therapeutic implications. *Circulation* **116**, 1832-1844 (2007).
39.   Zelisko, M., Li, J., & Sharma, P. What is the mechanism behind biological ferroelectricity? *Extreme Mechanics Letters* **4**, 162-174 (2005).
40.   Liu, Y., Wang, Y., Chow, M. J., Chen, N. Q., Ma, F., Zhang, Y., & Li, J. Glucose suppresses biological ferroelectricity in aortic elastin. *Physical Review Letters* **110**, 168101 (2013).
41.   Leuchtag, H. R., & Bystrov, V. S. Theoretical models of conformational transitions and ion conduction in voltage-dependent ion channels: Bioferroelectricity and superionic conduction. *Ferroelectrics* **220**, 157-204 (1999).

ACKNOWLEDGEMENTS

AUTHOR CONTRIBUTIONS

J.Y. Li and H.R. Zheng conceived and designed the projects. X.Y. Liu and F. Yan performed the experiments. L.L. Niu and Q.N. Chen performed data analysis. J.Y. Li, X.Y. Liu, and F.Yan wrote the paper. X.Y. Liu and F. Yan contributed equally to this work.

COMPETING FINANCIAL INTERESTS

The authors declare no competing financial interests.

Table 1 The analysis of variance (ANOVA) of peak value and mean value of corrected PFM amplitude (A_m) and resonant frequency (F_r) in four different groups of samples.

	1 (n = 12)	2 (n = 12)	3 (n = 12)	4 (n = 12)	F value	p value
Peak value (A_m)	$4.73\pm0.38^{*\#}$	$7.44\pm0.27^{\$@}$	$12.80\pm0.74^{\wedge}$	$19.48\pm2.71^{\&}$	250.27	< 0.001
Peak value (F_r)	$319.19 \pm 4.33^{\#}$	$316.81 \pm 3.85^{@}$	$314.73 \pm 4.47^{\wedge}$	$325.20 \pm 4.17^{\&}$	13.86	< 0.001
Average value (A_m)	$4.67 \pm 0.49^{*\#}$	$7.92 \pm 0.29^{\$@}$	$13.00 \pm 0.85^{\wedge}$	$19.42 \pm 2.31^{\&}$	310.08	< 0.001
Average value (F_r)	319.37 ± 5.21	$317.20 \pm 3.98^{@}$	$315.84 \pm 6.32^{\wedge}$	323.52 ± 4.50	5.25	0.003

Note: $*p < 0.05$ for 1 vs 2; $\#p < 0.05$ for 1 vs 3; $\&p < 0.05$ for 1 vs 4; $\$p < 0.05$ for 2 vs 3; $@p < 0.05$ for 2 vs 4; $^{\wedge}p <0.05$ for 3 vs 4.

Table 2 The analysis of variance (ANOVA) of coercive voltage in four different groups of samples

	1 (n = 46)	2 (n = 40)	2 (n = 31)	4 (n = 40)	F value	P value
Coercive voltage (V)	$2.80 \pm 1.75^{*\#}$	$8.60 \pm 2.43^{\$@}$	$19.82 \pm 7.42^{\wedge}$	1.42 ± 0.74	180.77	< 0.001

Note: $*p < 0.05$ for 1 vs 2; $\#p < 0.05$ for 1 vs 3; $\$p < 0.05$ for 2 vs 3; $@p < 0.05$ for 2 vs 4; $^{\wedge}p < 0.05$ for 3 vs 4.
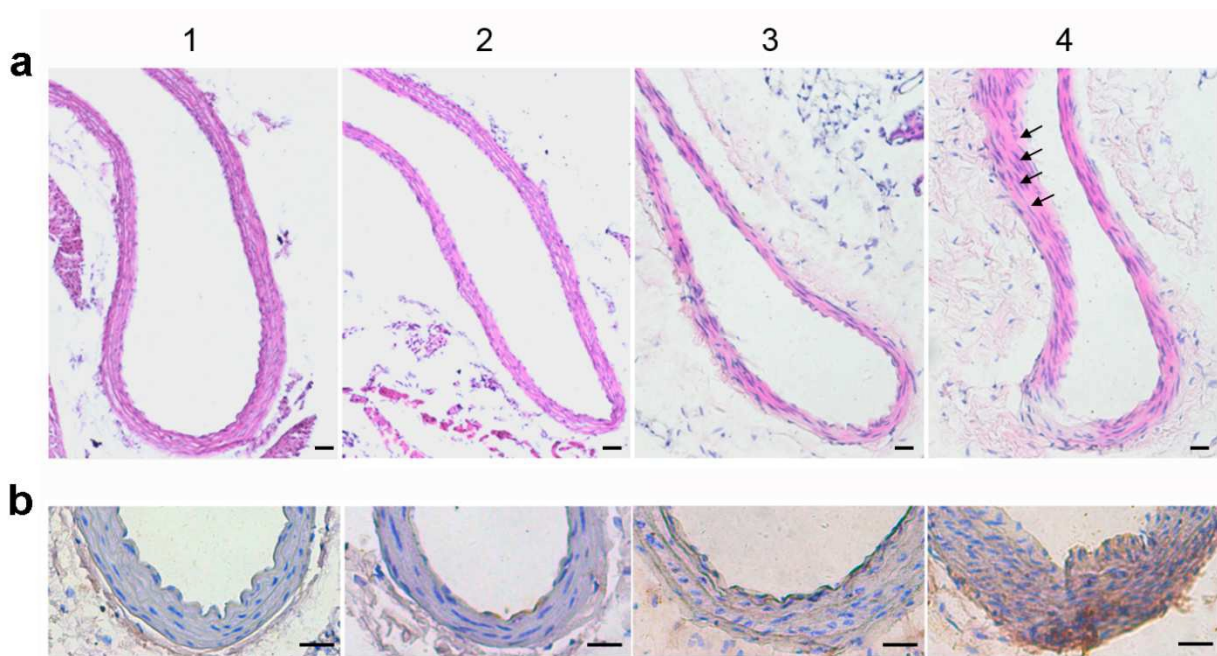
Figure 1 Histological analysis of the aorta from different groups of mice, with scale bar being 100 μm. (a) Representative hematoxylin and eosin (H&E) staining images. (b) Representative images from immunohistochemical staining with anti-a-smooth muscle actin antibody. Group 1 for the aortal samples from wide type mice, group 2 from APoE-/- mice fed with chow diet, group 3 for the plaque-free region 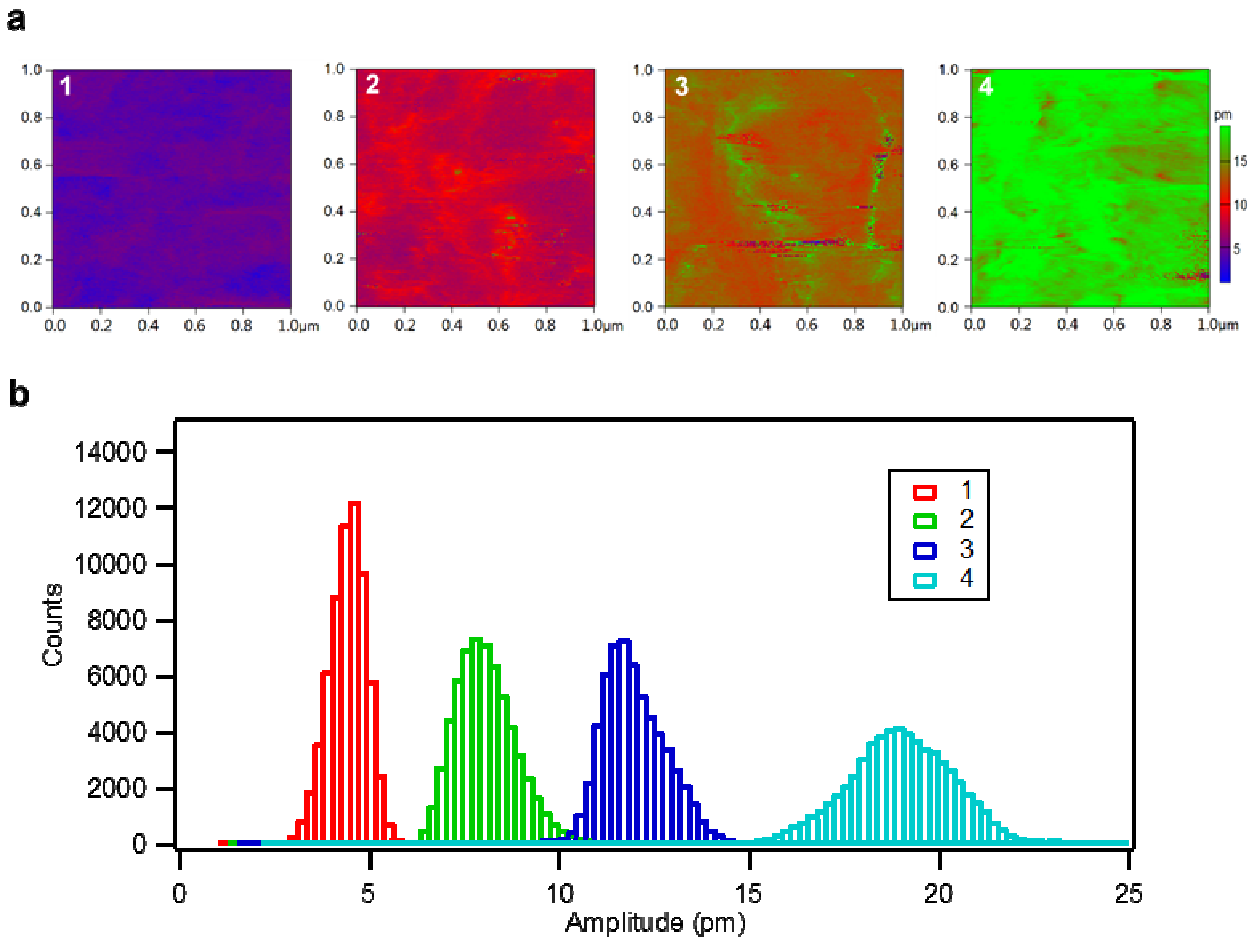of the aorta sample from APoE-/- mice fed with high fat diet, and group 4 for plaque region of the aorta sample from APoE-/- mice fed with high fat diet.

a

b

Figure 2 Comparison of PFM amplitude of four different groups of mouse artery tissues. (a) PFM amplitude mappings corrected using damped driven harmonic oscillator model. (b) Histogram of corrected PFM amplitude distributions.
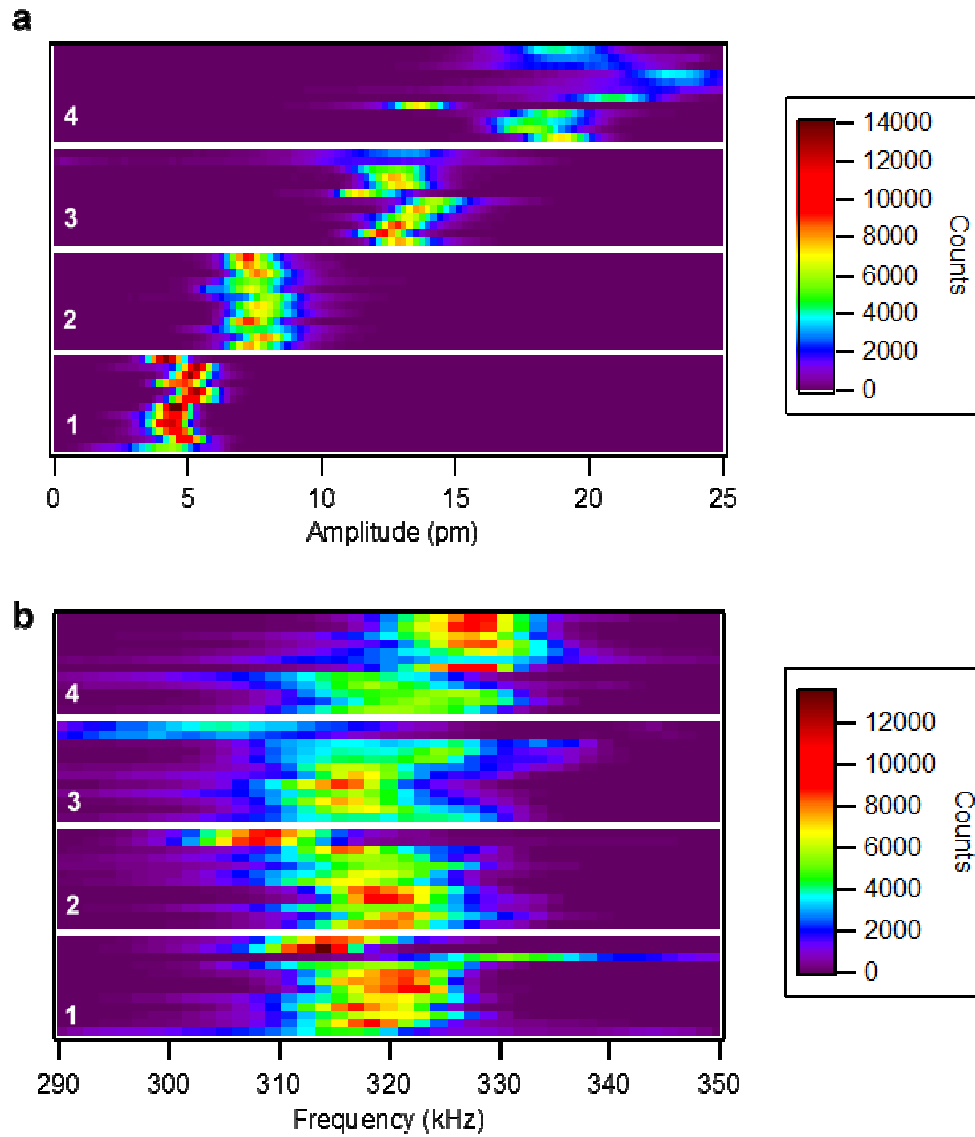
Figure 3 Distribution of histograms of four different groups of aorta samples ordered from bottom to top. (a) Corrected amplitude. (b) Resonant frequency.
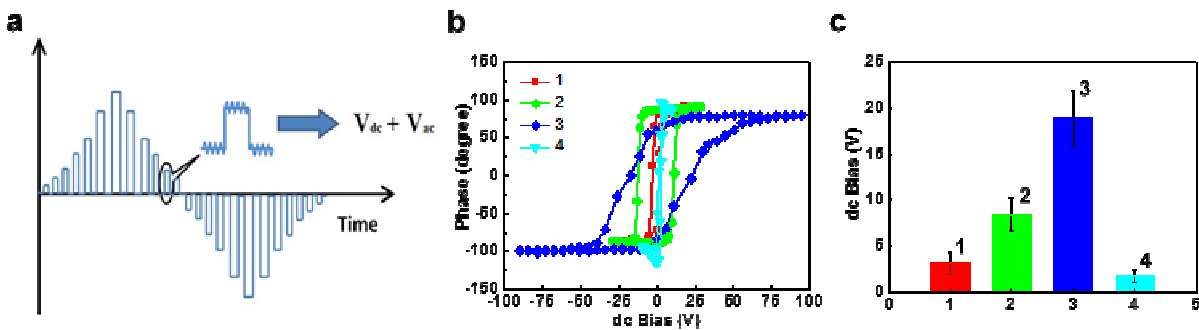
Figure 4 Comparison of coercive voltage of four different groups of samples. (a) Schematics of switching PFM. (b) Typical hysteresis loops. (c) Bar column comparison of coercive voltages.

Supplementary Materials

Materials and Methods

Animal model. Male wild type (wt) and APoE-/- mice in C57BL/6J background at the age of 8 weeks were obtained from Vital River Laboratory Animal Technology Co., Ltd. (Beijing, China). APoE-/- mice were fed with either a regular chow or a high-fat diet contained 21% fat and 0.15% cholesterol [34] for 24 weeks. In parallel, C57BL/6J mice fed with a chow diet for the same time as a control. All animal procedures were performed in compliance with the relevant laws and institutional guidelines for the care and use of laboratory animals. The protocols were approved by the Committee on the Ethics of Animal Experiments of Shenzhen Institutes of Advanced Technology, Chinese Academy of Science.

Sample preparation. Mice were anesthetized by intraperitoneal injection of 10% chloral. The mice were sacrificed, dissected and aortas were perfusion-fixed with 4.5% formaldehyde. After that, the aortas were dissected and fixed in 4% paraformaldehyde solution for 24 h. Oil red O staining was used to determine the atherosclerotic area on entire aortas. In brief, after removing surrounding adventitial fatty tissue, the aorta was rinsed in 70% ethanol, stained with 0.05% oil red O solution in 50% acetone/35% ethanol for about 10 min, and washed in 80% ethanol for 5 min. In order to avoid the interference of Oil red O in the PFM detection, the aortas were opened longitudinally and Oil red O dye was removed by decolorizing the aortas with 100% ethanol for 30 min. Then the aortas were washed with a graded ethanol/HMDS series: 30%, 50%, 70%, and 100% for 15 min each, and finally allowed to dry overnight.

Histochemical staining. The aorta samples were fixed by immersion in 4% paraformaldehyde for 24 h and embedded in paraffin. The sections (5 μm thick) were cut with a cryostat microtome (CM1950; Leica, Heidelberg, Germany). The paraffin-embedded sections were placed on poly-L-lysine-coated slides and immersed the slide in H_2O for 30 s with agitation by hand, following by dipping the slide into a Coplin jar containing Mayer's hematoxylin for 30 s. Then the slide was rinsed in H_2O for 1 min. After that, the slide was stained with 1% eosin Y solution for 10-30 s with agitation. After the sections were dehydrated with two changes of 95% alcohol and two changes of 100% alcohol (each change for 30 s), one drop of mounting medium was added and

covered with a coverslip. Aorta sections were viewed under a light microscope (Olympus BX43 microscope, Olympus, Tokyo, Japan).

Immunohistochemistry. For the expression analysis of α-SMA, tissues prepared from paraffin-embedded samples were immunohistologically stained with goat anti-α-smooth muscle actin antibody (1:50 dilution, Santa Cruz) anti-α smooth muscle actin antibody, followed by further staining with rabbit anti-goat secondary antibodies (1:100 dilution; BD Biosciences). Cell nuclei were counterstained by hematoxylin (1:100 dilution; Invitrogen). Tissue sections were viewed under a light microscope (Olympus BX43 microscope, Olympus, Tokyo, Japan).

PFM experiment. Asylum Research MPF-3D atomic force microscope was used for PFM studies. The probe was made by silicon, with the lever and the tip coated with Ti/Ir (5/20), and the radius of tip is 28 ±10 nm. The resonance frequency of the lever in air is 70 kHz and the spring constant of lever is 2 N/m. During the switching PFM, two cycles of DC bias were applied, starting from negative maximum towards to the positive one, with the period set to be 5 s and each "on" and "off" steps maintained at 50 ms. All the data shown in the paper were obtained in the second cycle.

Statistical analysis. All data were evaluated by the PASW Statistics 18. p less than 0.05 was considered statistically significant. Parametric data was expressed as mean ± standard deviation. A comparison of the amplitude, resonant frequency and dissipation for the different groups was made by analysis of variance (ANOVA).
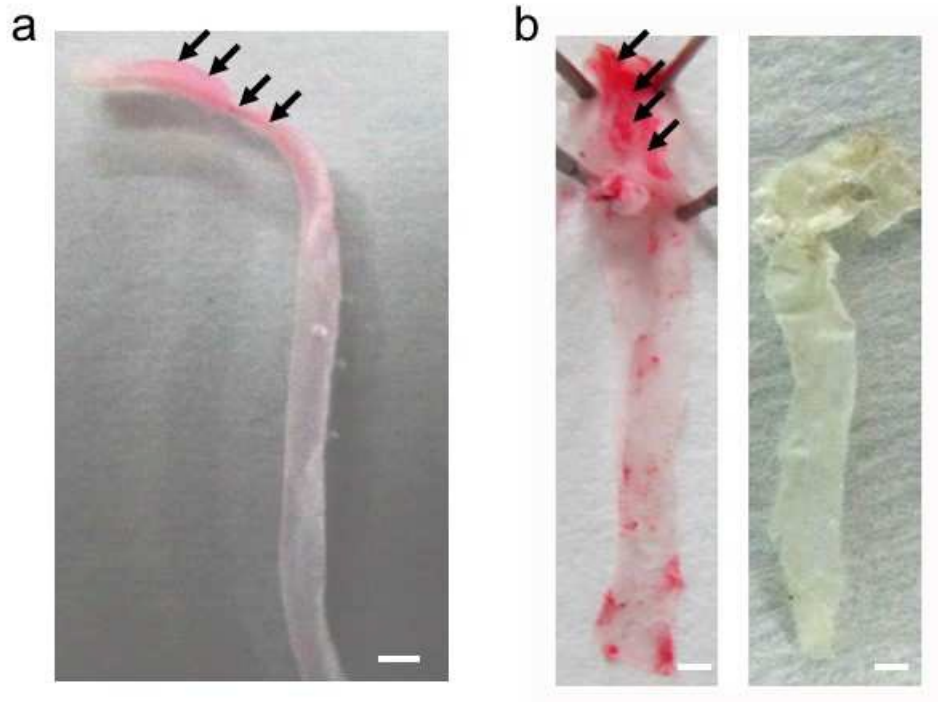
Figure S1 Localization of atherosclerotic area by oil red O staining. (a) A representative picture showing the atherosclerotic area after oil red O staining. (b) Representative en face atherosclerotic aorta preparations stained with oil red O (left), and followed by decolorization and dryness (right). Arrows: plaque sites, bar scale: 1 mm.
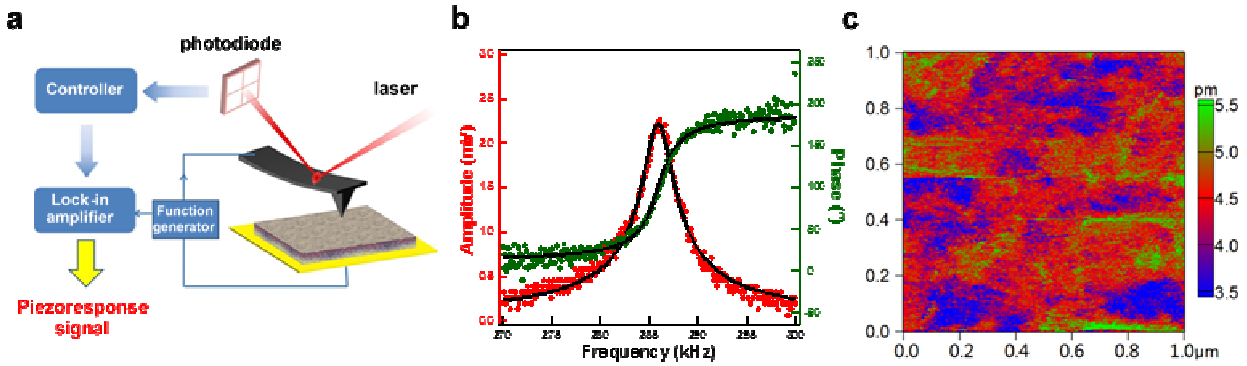
Figure S2 The concept of PFM. (a) Schematic of PFM. (b) Resonance-enhanced PFM, wherein phase and amplitude versus driving frequency can be fitted by damped driven harmonic oscillator model for quantitative analysis. (c) A typical PFM amplitude mapping of normal artery tissue of C57BL/6J mouse fed with a chow diet, corrected using damped driven harmonic oscillator model.
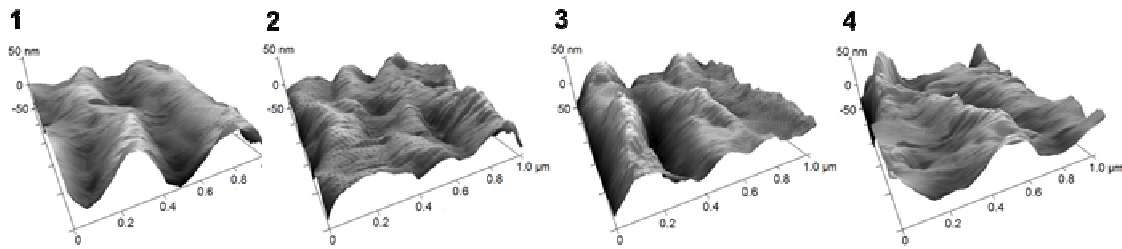

Figure S3 3D SPM topographic images of four different groups of mouse artery tissues.
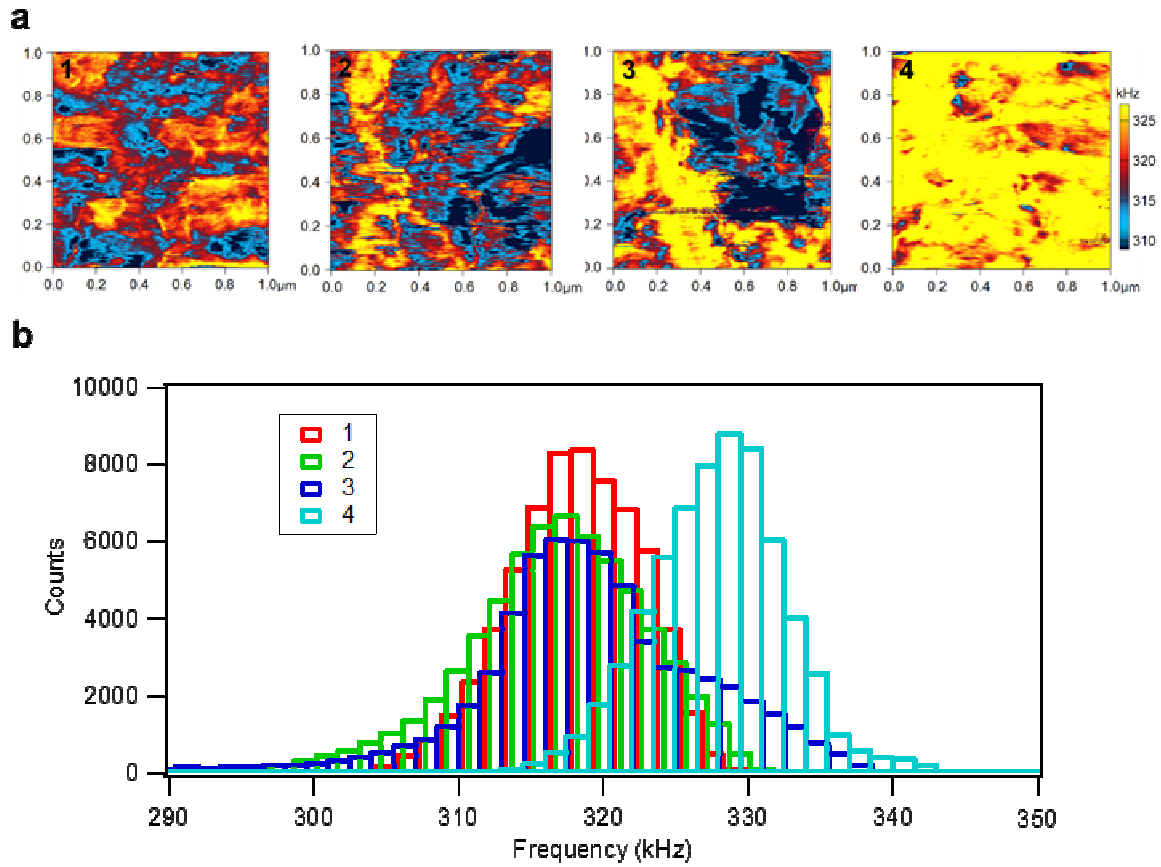
Figure S4 Comparison of resonant frequency of four different groups of mouse artery tissues. (a) Resonant frequency mappings calculated using damped driven harmonic oscillator model. (b) Histogram of calculated resonant frequency distributions.
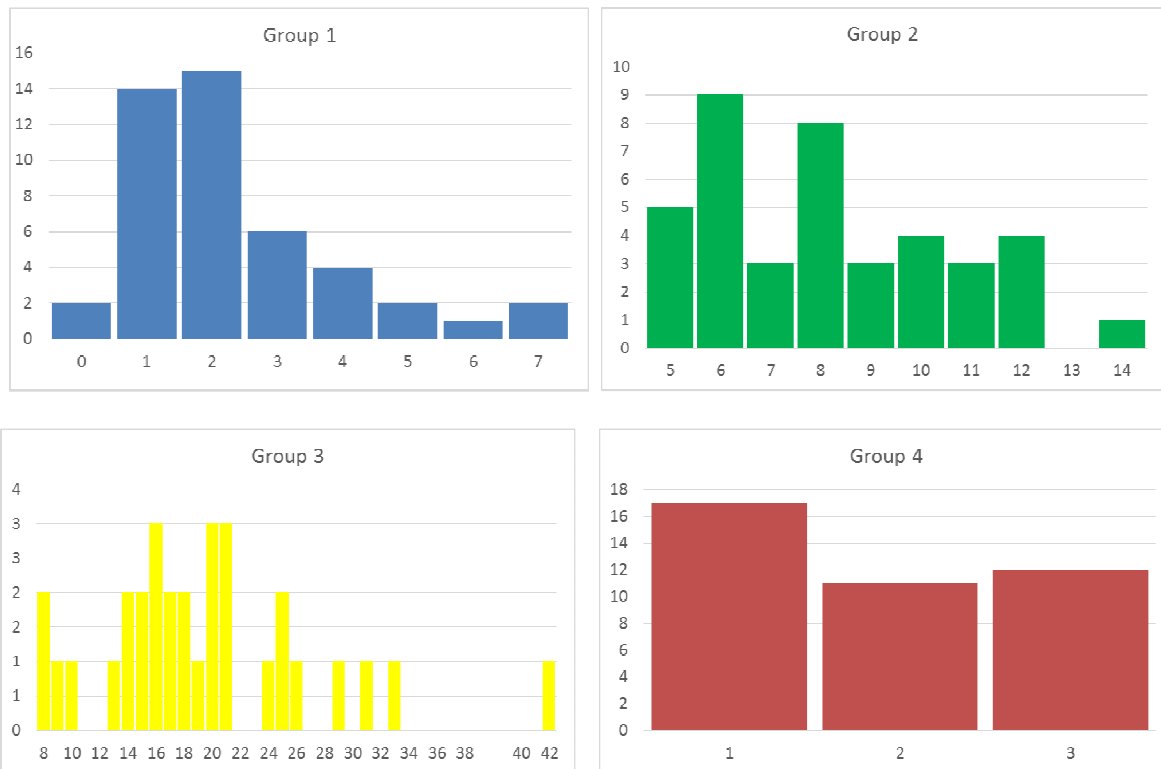
Figure S5 The histogram distributions of coercive voltage for the four groups of samples, where the difference among different groups is evident. The horizontal axis is coercive voltage, while the vertical axis is the count of occurrence.